Tellus SERIES A DYNAMIC METEOROLOGY AND OCEANOGRAPHY
PUBLISHED BY THE INTERNATIONAL METEOROLOGICAL INSTITUTE IN STOCKHOLM

Structure and variability of the Oman coastal low-level jet

By RAZA RANJHA[1,2,3]*, MICHAEL TJERNSTRÖM[1,2], ALVARO SEMEDO[4,5], GUNILLA SVENSSON[1,2] and RITA M. CARDOSO[5], [1]*Department of Meteorology, Stockholm University, Stockholm, Sweden*; [2]*Bolin Center for Climate Research, Stockholm University, Stockholm, Sweden*; [3]*Department of Physical Geography and Ecosystem Science, Lund University, Lund, Sweden*; [4]*CINAV-Escola Naval, Lisbon, Portugal*; [5]*Faculdade de Ciências, Instituto Dom Luiz, University of Lisbon, Lisbon, Portugal*

(Manuscript received 25 June 2014; in final form 19 May 2015)

ABSTRACT

In this study, reanalysis and regional atmospheric modelling was used to resolve the climatology and mesoscale structure, spatial variability and temporal characteristics of the Oman coastal low-level jet (CLLJ). The limited area model COAMPS® was used at a 6-km horizontal resolution for a 5-month period (May–September) during 2009. Analysis of high-resolution model fields reveals the mesoscale structure of the Oman CLLJ, clearly distinguishing it from the large-scale South Asia monsoon circulation farther offshore, and from the previously identified Findlater (or Somali) jet, which occurs at a higher altitude. The Oman CLLJ is closer to the coast and spreads northeastward along the coast of Oman, clearly interacting with the coastal topography and headlands. It has a very strong annual cycle, related to the South Asia monsoon, with July exhibiting the highest CLLJ frequency of occurrence (around 80%) and highest wind speeds (around 27 ms^{-1}), and May and September being the transition months. The southerly location of the Oman CLLJ, along with the very strong inland summer heating in the Arabian Peninsula, affects its diurnal cycle, with highest number of occurrences early in the morning, whereas the highest wind speeds occur during late afternoon, setting this CLLJ apart from other coastal jets in mid-latitude areas along eastern boundary currents.

Keywords: boundary layer meteorology, mesoscale meteorology, climate modelling, climatology, low level jet, coastal jet, dynamic downscaling

1. Introduction

Coastal low-level jets (CLLJ) are coast-parallel winds, with significant wind-speed maxima in the vertical, confined to the marine atmospheric boundary layer (MABL) typically within ~1000 m or less from the surface. Although CLLJs have a relatively small vertical extent, their horizontal width can exceed hundreds of kilometres off the coast, typically limited by the Rossby radius of deformation. Ranjha et al. (2013) showed that CLLJs can be found along mid-latitude west coasts of every continent, except Antarctica. However, they also found a CLLJ at an easterly coast, along the southeast (SE) coast of the Arabian Peninsula, most pronounced along the coast of Oman and previously poorly documented, which is the topic of this study.

So far the most studied CLLJ is the California coastal jet, along the north and central west coast of the USA, mainly along the coasts of Oregon and California. Numerous observational and modelling studies have been pursued there (e.g. Chao, 1985; Burk and Thompson, 1996; Cui et al., 1998; Ström et al., 2001; Rahn and Parish, 2007). Zemba and Friehe (1987) examined the MABL structure along the California coast and concluded that the thermal wind structure caused by strong land–sea temperature contrast is fundamentally responsible for the existence of a CLLJ there. Beardsley et al. (1987) highlighted the diurnal variability of the California CLLJ, showing that it has a maximum wind speed somewhere during late afternoon to early evening and weakens through the night, with the lowest wind speeds occurring early morning. The role of coastal topography and its orientation for local enhancements of the flow speed were also emphasised in several studies (e.g. Parish, 1982; Winant et al., 1988; Burk and Thompson, 1996; Tjernström, 1999; Tjernström and Grisogono, 2000). This coastal jet has hence become the prototype for CLLJ studies around other regions.

CLLJs are important for coastal weather along mid-latitude west coastal areas and have implications for aviation, shipping, commercial fishing, pollutant and aerosol

*Corresponding author.
email: razaranjha@gmail.com; ranjha@misu.su.se

Citation: Tellus A 2015, **67**, 25285, http://dx.doi.org/10.3402/tellusa.v67.25285

dispersion, off-shore wind power, as well as for several other human activities. The presence of CLLJs also modifies the vertical wind shear and consequently the turbulence structure within the MABL, thus playing an important role in the mixing and transport processes in the lower atmosphere (Beardsley et al., 1987; Nuss et al., 2000). The spatial distribution of coastal winds is also closely linked to the nature of coastal fog and stratus cloud cover (Nuss et al., 2000). While large-scale subsidence and boundary-layer turbulence are important in determining the summertime distribution of stratus cover (Brost et al., 1982; Tjernström and Koracin, 1995), the low-level coastal winds are equally vital (Koracin and Dorman, 2001). Coastal winds exert stress on the ocean surface, displacing coastal waters offshore by Ekman transport which, bringing colder deep waters to the surface due to upwelling, set favourable conditions for the formation of fog or low clouds.

The cold and nutrient-rich upwelling water is also important for the marine ecology and the fishing industry, hence the coasts adjacent to upwelling regions are usually among the most inhabited and productive regions in the world (Small and Nicholls, 2003). Upwelling alters the sea-surface temperature (SST) pattern along the coast by lowering the ocean temperature, and consequently, intensifies the land–sea temperature, and hence pressure gradient, strengthening the wind speed and CLLJ occurrences through positive feedback along the coast (Rijo et al., 2014; Soares et al., 2014). This decrease of SST along the coast also lowers the ocean surface evaporation, which combined with the strong coast-parallel winds, limits the onshore moisture advection and contributes to the aridity and dryness of some of the mid-latitude western coastal regions (Warner, 2004).

As shown by Ranjha et al. (2013), almost all CLLJ regions have a characteristic facilitating large-scale synoptic forcing: a high-pressure system over the ocean (the semi-permanent subtropical highs) and a thermal low inland. The seasonal appearance of the CLLJ is determined by the meridional migration of the sub-tropical high and the strength of the inland heating. One prominent exception found in the global CLLJ climatology is the coastal jet along the SE coast of the Arabian Peninsula, where the South Asia monsoon circulation plays the same role as the sub-tropical high-pressure circulation does along mid-latitude continental western coasts. This CLLJ is unique in the sense that it is located along the eastern side of a continent, the SE coast of Oman, and exhibits the globally highest CLLJ occurrence rate during its peak season: around 70% (Ranjha et al., 2013). This coastal jet has a strong seasonality with most occurrences during boreal summer (July–August: JJA), whereas it is totally absent during the boreal winter (Ranjha et al., 2013). The Arabian Sea is subject to large-scale seasonal atmospheric circulation reversals. During the boreal winter, it is under the influence of relatively cool, dry and moderate northeasterly (NE) winds, whereas the wind-direction reverses during JJA (the summer monsoon season), with strong southwesterly (SW) winds, favouring coast-parallel flow along the Arabian Peninsula in the Arabian Sea region. The summer monsoon steams from the seasonal development of a (thermal) low-pressure area over the Asian land mass and a high pressure area over the southern Indian Ocean (the Mascarene High), and accounts for roughly half of the global inter-hemispheric transport of air in the lower troposphere (Findlater, 1969a, 1969b). Associated with the summer monsoon is the Findlater or Somali low-level jet (Findlater, 1969a), with strong and persistent SW wind across the Arabian Sea.

Since the discovery of the Findlater jet, the role of the southern hemisphere circulation for the South Asia summer monsoon has been the subject of several studies, and it is now well established that the large-scale wind pattern over the Arabian Sea is responsible for the moisture transport and consequent monsoon precipitation in South Asia (Pant and Kumar, 1997; Webster et al., 1998; Houze et al., 2007; Ullah and Gao, 2012). Findlater (1971), using monthly-mean winds, showed that the Findlater jet splits into two branches, one passing eastwards over India and the other southeastwards towards Sri Lanka (see Fig. 1 in Findlater, 1971). However, the wind speeds are intensified at the coast, primarily due to the cross-coast baroclinicity generated by the sharp land–sea thermal contrasts, and the Oman CLLJ is also considerably shallower than the Findlater jet. Although it has been known for some time that high winds are common off the coast of Oman, mostly from the operational meteorology community (COMET, 2004), the existence of a CLLJ there was first documented by Ranjha et al. (2013), based on an analysis of data from the coarse-resolution ERA-Interim reanalysis (Dee et al., 2011) from the European Centre for Medium-Range Weather Forecasts (ECMWF).

The small-scale structure and dynamics of the Oman CLLJ could not be properly studied from ERA-interim by Ranjha et al. (2013) due to its coarse resolution. Thus, this is the aim of the present paper, using high-resolution regional simulations with the Coupled Ocean/Atmosphere Mesoscale Prediction System (COAMPS®, Hodur, 1997). The paper is organised as follows: Section 2 describes the data and the model setup, Section 3 depicts the synoptic conditions, Section 4 describes the characteristics of the Oman coastal jet, and finally Section 5 presents the summary and conclusions.

2. Data and the model setup

The atmospheric component of the COAMPS® mesoscale model (Hodur, 1997) was used to provide high-resolution three-dimensional regional fields in the area of interest. The COAMPS® model solves the finite-difference

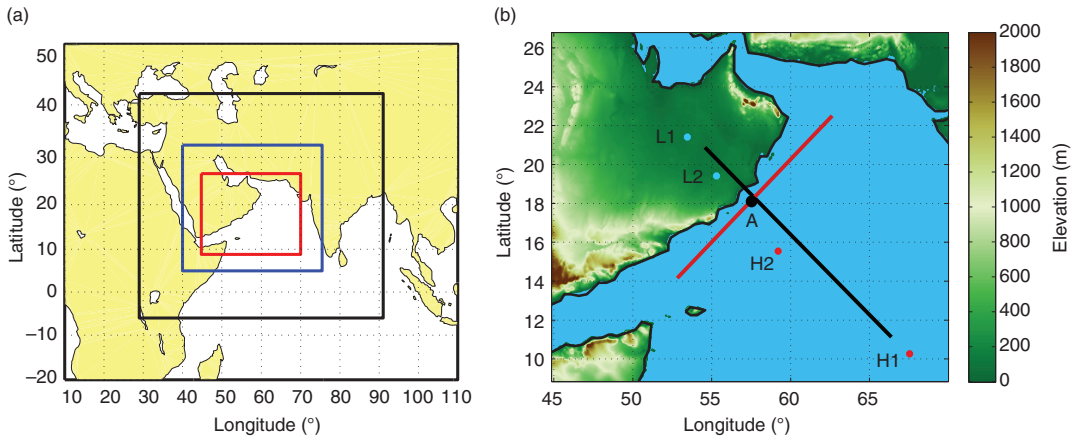

Fig. 1. (a) COAMPS® domains used in the downscaling, from outermost to innermost domain with horizontal resolution of 54 km (black line), 18 km (blue line) and 6 km (red line), respectively, and (b) inner domain, with topography height contours, showing the key points L1 and H1, and L2 and H2 (see Figs. 14 and 15), and A (CLLJ point as black dot at 18°N, 57°E), and the cross-section lines for cross-coast (black line) and along-coast (red line) used in Fig. 8.

approximation of the fully compressible, non-hydrostatic equations on an Arakawa C-grid, using a height-based terrain-following vertical σ_z coordinate. Parameterisations for short- and long-wave radiation, surface fluxes, cumulus convection, boundary layer turbulence (using a level 2.5 turbulence scheme), and moist processes (including micro-physical quantities) are discussed in Hodur (1997) and Hodur and Doyle (1999).

ERA-Interim reanalysis data were used as 6-hourly lateral boundary forcing fields, while the SST was updated every 24 hours, using the Global Ocean Data Assimilation Experiment (GODAE) high-resolution SST (GHRSST) data (Donlon et al., 2007). The domain configuration for the COAMPS® model simulation is shown in Fig. 1, and comprises three one-way nested domains, with horizontal resolutions of 54 km, 18 km, and 6 km, respectively (Fig. 1). Figure 1b depicts the innermost domain, with key synoptic and mesoscale points (H1 and L1, H2 and L2, and A, respectively), as well as the topographic height contours over land. The model was configured with 51 vertical levels on a non-uniform vertical grid, with 14 model levels within the lowest 2 km and the lowest level at around 8 m.

The analysis is performed for a representative year (2009) for May through September period, covering the South Asia summer monsoon season (June–August) and the transition months. To provide sufficient time for model spin up, the simulation was started on 25th April 2009. The 5 months analysis period, from 1st May through 30th September, 2009, will hereafter be referred to as MJJAS.

Reanalysis data have become an important tool for studying global as well as regional climate, especially in regions where observations are sparse or infrequent. In the current study the ERA-Interim reanalysis, in addition to providing lateral boundary conditions, provided the climatological background. The horizontal resolution utilised is $1^\circ \times 1^\circ$ with 60 vertical model levels. The choice of using this reanalysis is based on its ability to represent large-scale wind patterns, as well as to resolve some local-scale features. A comparison between QuikSCAT and ERA-Interim 10-m winds (Collins et al., 2012), showed good overall agreement over the western tropical Indian Ocean. Furthermore, Collins et al. (2012) compared NCEP-NCAR (Kalnay et al., 1996) and the ERA-Interim reanalyses for the Indian Ocean region and concluded that small-scale wind features associated with orographic effects are more faithfully represented in ERA-interim. Similarly, Annamalai et al. (1999) studied the mean evolution and variability of the South Asia summer monsoon and also concluded that the ERA-Interim is superior to the NCEP-NCAR reanalysis in terms of the seasonal mean climatology. They also found that the Findlater Jet extends further north, over the Arabian Sea and into northwestern (NW) India, in ERA-Interim than in the NCEP reanalysis, where it is more zonal.

3. Synoptic conditions

The boreal summer Indian Ocean large-scale pressure gradients and low-level atmospheric circulation are presented in Fig. 2, showing the seasonally averaged fields of mean sea-level pressure (MSLP), and the wind speed close to the surface and at $\sim$400 m a.s.l. from ERA-Interim, for the years 1980–2011. The 400 m altitude is chosen as, roughly, the representative height of the CLLJ wind-speed maxima (Ranjha et al., 2013). The low pressure over continental Asia, as well as the high-pressure cell over the southern Indian Ocean, is clearly visible (Fig. 2a), as is the

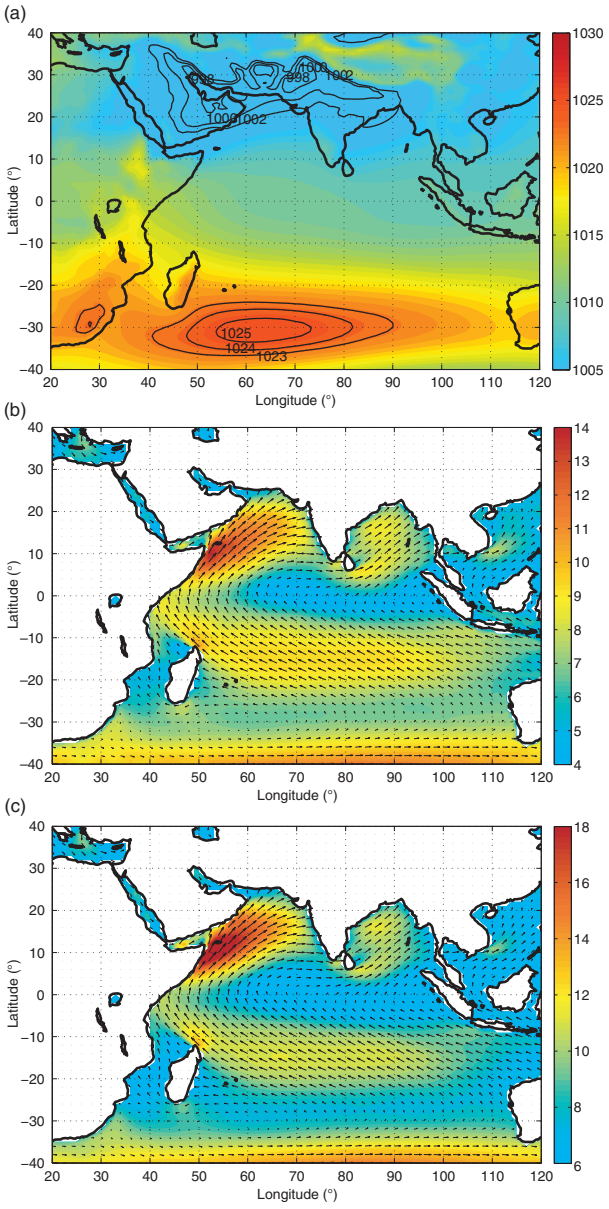

Fig. 2. Seasonal averages (JJA) from ERA-Interim of (a) MSLP (hPa), (b) wind speed at the lowest level (~25 m) and (c) wind speed at ~400 m a.s.l. (m s^{-1}) with arrows representing the wind direction. Note the differences in colour scale between panels b and c. The data are from the period 1980–2011.

cross-equatorial pressure gradient that preconditions the large-scale wind pattern associated with the Findlater Jet (Fig. 2b). The low-level atmospheric circulation and overall synoptic pattern of the low-level jet discussed by Findlater (1969a) are noticeable in the seasonal mean fields captured by ERA-Interim. The south Indian Ocean trade winds are seen crossing the equator close to the east African coast, turning clockwise towards SW winds over the Arabian Sea as a consequence of the northern hemisphere Coriolis deflection. This large-scale wind pattern is noticeable both at the surface and at ~400 m (Fig. 2b and c). Temporal variations in strength and position of this system steer the annual cycle of the atmospheric circulation in the Arabian Sea, and influence the monsoon regime. The surface-wind features identified by Findlater (1969a) in the vicinity of the northern tip of Madagascar are also resolved fairly realistically in the ERA-Interim, in agreement with the island-corner accelerations noted by Risien and Chelton (2008).

Since the large-scale forcing that preconditions the summer monsoon and the Findlater jet is evident in considerable detail from Fig. 2, the ERA-Interim reanalysis data were thus subjected to the CLLJ detection algorithm proposed by Ranjha et al. (2013), to obtain a monthly CLLJ climatology for a 31-yr period (1980–2011). The reanalysis data were also filtered separately for 2009, the representative year selected for the detailed analysis in the present study. The algorithm detects the CLLJ wind-maxima height, wind speed and direction, here presented for an area roughly coinciding with the COAMPS® innermost domain (see Fig. 1b). The objective is to determine the monthly variations in the CLLJ pattern and to justify the choice of 2009 for the modelling analysis, based on a comparison with the long-term climatology.

Figure 3 shows the monthly mean-maximum CLLJ frequency of occurrence and the monthly mean of maximum wind speeds when CLLJs occur, for each month (January to December) along the coast of Oman, for 2009 and for the 31-yr climatology. It is clear from the latter (Fig. 3b) that CLLJs are most frequent during JJA, whereas May and September can be regarded as transition or onset and decline months, respectively. In terms of frequency of occurrence, 2009 (Fig. 3a) appears to be consistent with the 31-yr climatology, with a correlation coefficient of 0.94. Similarly, the highest CLLJ wind speeds also occur during summer, consistent with the highest frequencies of occurrence, with the corresponding decline starting in September, while May represents the beginning of increased wind speeds in this area (Fig. 3c and d). A reasonable agreement can be seen between the monthly results for 2009 (Fig. 3c) and the 31-yr climatology (Fig. 3d), with a correlation coefficient of 0.97, indicating also that in terms of wind speed, 2009 can be considered a typical year. In general this pattern is consistent with the large-scale atmospheric circulation and the onset and decline periods of the corresponding South Asia monsoon as discussed by Findlater (1969a). Since the 2009 statistics compare well with the general climatology in this area, this was the year selected for the COAMPS® regional modelling simulations.

In the absence of conventional measurements in the area, a brief model evaluation was performed with a product based mostly on remote sensing observations. The COAMPS® near-surface wind speeds (at 8 m a.s.l.) from the innermost

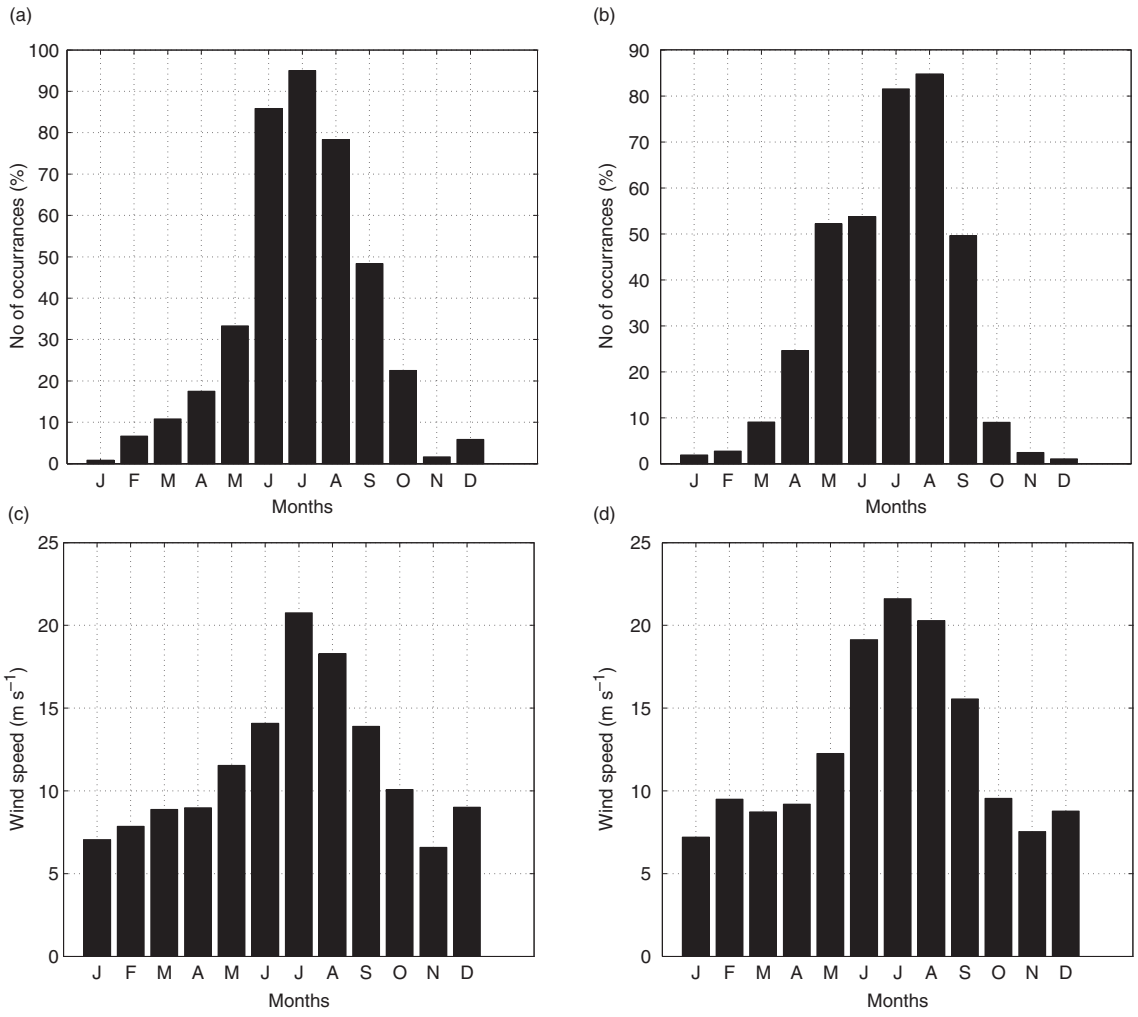

Fig. 3. Monthly mean maximum CLLJ frequencies of occurrence (%) for each month from ERA-Interim for an area coinciding with the inner modelling domain (see Fig. 1b) for (a) 2009, and (b) 1980–2011, and monthly mean of maximum wind speeds when CLLJs occur, for the same area, also from ERA-Interim, for (c) 2009, and (d) 1980–2011 (m s^{-1}).

domain were compared to the Cross-Calibrated Multi-Platform (CCMP) ocean surface wind vector analyses (Atlas et al., 2011). The CCMP is an over 20 yr long, 25 km resolution, ocean-surface wind dataset, produced using a variational analysis method to combine extensive cross-calibrated multiple satellite datasets with in situ observations and ECMWF analysis. However, these results should be used with caution since remotely sensed wind speeds along ocean current systems, particularly close to the coast, have accuracy problems (Atlas et al., 2011). Therefore, in many CLLJ areas CCMP winds are prone to errors (Atlas et al., 2011; their Fig. 10). When computing the statistics a mask was applied to the Gulf of Aden, the Strait of Hormuz and the Persian Gulf, since these areas are affected by these coastal problems. For each remaining ocean grid point, the bias, correlation coefficient (r), mean absolute error (MAE), root mean square error (RMSE), and variability ratio (σ_m/σ_c, the ratio of the standard deviations of modelled, σ_m, to observed winds, σ_c) were calculated. The mean values of these statistics over the innermost domain are summarised in Table 1. Overall, the wind speed is well reproduced by the COAMPS® and the slight bias is well within the uncertainty of the observations. The RMSE and r are also acceptable, and the variability of the wind speed is well captured by the model, as shown by the variability ratio.

Several studies have shown that regions with high CLLJ occurrence have high upwelling rates, as a consequence of offshore Ekman transport triggered by the wind stress (e.g. Beardsley et al., 1987; Zemba and Friehe, 1987; Parish, 2000; Capet et al., 2004; Fennel and Lass, 2007). The Oman coast is no exception, and during summer upwelling is a dominant feature of the air–sea interaction in the north Arabian Sea (e.g. Currie, 1992; Izumo et al., 2008). Figure 4 shows the 2009 ERA-Interim monthly

Table 1. Error statistics of COAMPS® innermost domain surface wind speeds against CCMP winds

	Corr.	Bias (m/s)	MAE (m/s)	RMSE (m/s)	Stdev ratio
Wind speed	0.65	−1.0	2.5	3.08	1.05
u	0.69	−0.8	2.52	3.27	0.93
v	0.70	−0.9	2.17	2.85	0.95

mean wind speed annual cycle at the approximate jet height, ∼400 m a.s.l., and the corresponding monthly mean SST at a central location for the Oman CLLJ area (point A in Fig. 1b). During winter months the mean wind speed is lower (∼5 m s^{-1}), while the SST increases from February to May (from ∼26 to ∼28°C). During summer months, the wind speeds are the highest (∼14–15 ms^{-1}), while the SST is the lowest (∼25°C). Hence there is a clear relationship between the increase in the wind speed and the decrease in the SST at this location, most likely due to CLLJ induced upwelling. There is some time lag between the onset of higher wind speeds and the subsequent SST decrease. This delay can be explained with the time between the CLLJ formation and the consequent Ekman pumping/transport, due to the wind stress on surface waters, leading to upwelling thereby decreasing the SST. The time lagged correlation coefficient between the wind speed and the SST annual cycles shown in Fig. 4 is −0.91 (anti-correlation), with a delay of 1 month.

4. Characteristics of the Oman coastal jet

4.1. Case study of a CLLJ event

Typical vertical profiles of wind speed, temperature, and potential temperature for a particular CLLJ occurrence, on 2nd July 2009 at 20:00 local time (LT), from the innermost

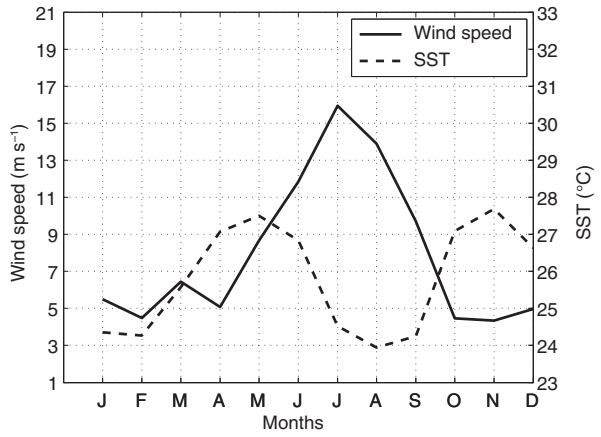

Fig. 4. Time series of monthly mean wind speed at ∼400 m a.s.l. (m s^{-1}) and SST (°C) for 2009, from ERA-Interim at point A (see Fig. 1b).

COAMPS® domain (at point A), are shown in Fig. 5. This CLLJ occurrence was detected by the identification criteria defined by Ranjha et al. (2013). From the wind-speed profile (Fig. 5a) a wind-speed maximum is clearly visible at ∼400 m a.s.l., and a sharp decrease in wind speed at higher altitudes is also evident, which satisfies the basic criterion for the presence of a CLLJ. However, to fully qualify as a CLLJ, the temperature profile also needs to fulfil the supplementary criterion of having an inversion at or around the nose of the jet. The temperature profile inversion is seen also at ∼400 m a.s.l. (Fig. 5b). It is interesting to note, however, that the potential temperature profile (Fig. 5c) does not provide any strong guidance to the presence of an inversion corresponding to the CLLJ, as discussed by Ranjha et al. (2013). Instead the boundary layer below the jet is stably stratified with an almost constant stability, and the inversion is hardly even detectable (Fig. 5c). The profiles in Fig. 5a and b corroborate the presence of CLLJs along the coast of Oman and provide a basis for further investigations of their spatial structure and temporal variability, based on high-resolution modelling fields. The criteria discussed above are designed to capture the footprint of the physical mechanisms driving a coastal jet. The proximity to a coast, however, is not a criterion, as it would involve an assumption on the scale of the phenomenon. As shown by Ranjha et al. (2013) such a criterion is not necessary.

Dominant regional-scale features of a particular CLLJ event (also for 2nd July, 2009, 20:00 LT) are illustrated in Figs. 6 and 7, showing the horizontal structure of the wind and temperature fields for the innermost modelling domain from the COAMPS® simulation. In Fig. 6, where the horizontal fields of near-surface (at 8 m a.s.l.) temperature and MSLP are shown, strong baroclinicity can be seen offshore at around 18°N, 57°E, where the temperature contours are almost perpendicular to the pressure gradient. This pattern is similar to those found in earlier studies of CLLJs, and highlights the role of baroclinicity associated with horizontal temperature gradients (strongest at the coast) as an important factor for the formation and strength of low-level jets (Zemba and Friehe, 1987; Burk and Thompson, 1996; Holt, 1996; Parish, 2000). The baroclinicity extends northeastwards, whereas to the SW it decreases. The low-level air temperature offshore Oman in the Arabian Sea, particularly towards the Gulf of Oman, is considerably lower

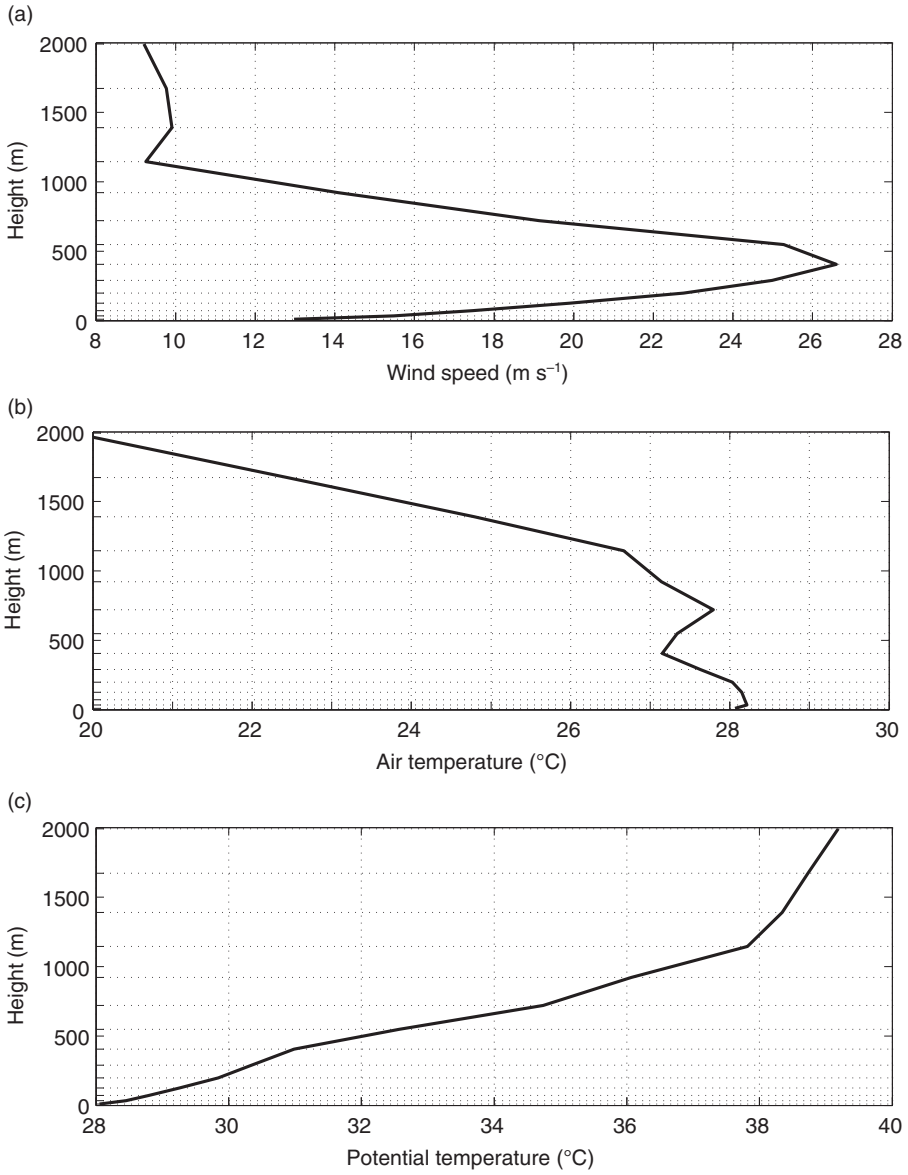

Fig. 5. Case-study vertical profiles from COAMPS®, of (a) wind speed (m s^{-1}), (b) temperature (°C), and (c) potential temperature (°C) at point A, on 2 July 2009 at 20:00 LT (16:00 UTC). Ticks on the y-axis and corresponding grid lines represent the model vertical grid spacing.

than the in-land temperature and its pattern is coherent with the SST (see Fig. 7c below). This strong land-sea temperature contrast gives rise to large cross-coast mesoscale pressure gradients, particularly close to shore. Figure 7 shows the horizontal fields of wind speed and wind direction at 8 m a.s.l. and at ~400 m a.s.l., and of the SST (the daily mean for 2nd July). A region of high wind speeds near the coast can be seen in the vicinity of the pronounced baroclinic structure (Fig. 7a and b). These winds are even stronger at 400 m a.s.l. (Fig. 7b) and extend northeastwards, consistent with the region of high baroclinicity.

The near-surface wind speed is weaker and also differs structurally compared to the wind field around the jet-core height. This is uncommon for CLLJs and may be one of the reasons why the Oman jet has gone relatively unstudied, that is, the surface observations do not clearly reflect the jet the same way they do in some other regions, for example in California. Also note the high wind speed aloft (Fig. 7b) appears in two distinct regions. First there is a high wind-speed area closely aligned with the coast of Oman and then, beyond this, a second, somewhat wider wind pattern further offshore to the south. The latter originates from the Horn

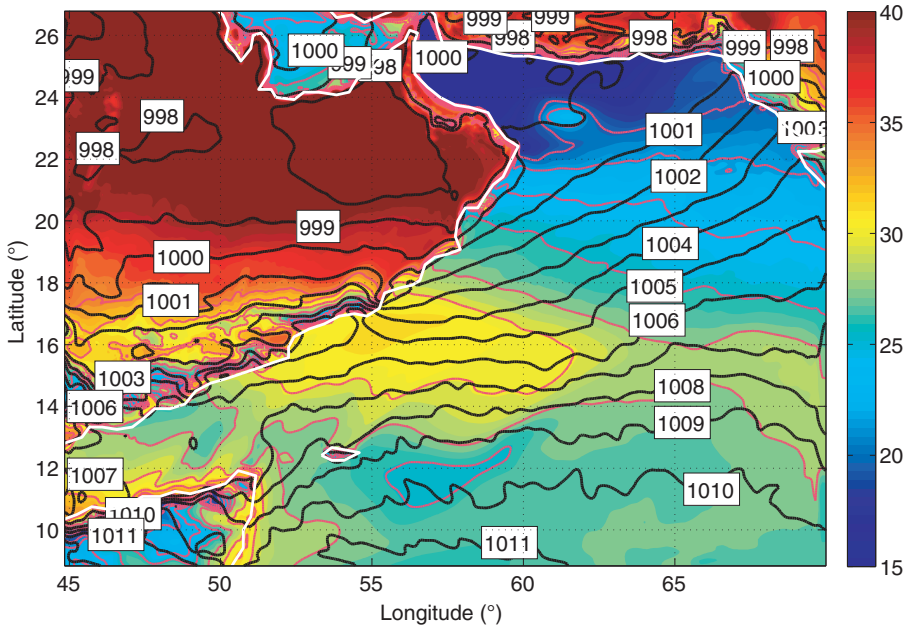

Fig. 6. Case-study horizontal fields from COAMPS® (2 July 2009 at 20:00 LT– 16:00 UTC) of temperature at 8 m (°C; background field and red lines) and MSLP (black lines with labels).

of Africa and extends all the way towards the Indian coast across the Indian Ocean, while the former has a more coast parallel pattern and is directed more towards the coast of Pakistan. Hence at this resolution, the distinction between the Oman CLLJ and the Findlater jet, not clearly present in ERA-Interim winds, becomes clear.

The high resolution SST field (GHRSST, see above), used for forcing the COAMPS® model simulations, is shown in Fig. 7c. Two distinct temperature zones are seen along the coast of Oman, separated by a rather sharp, almost east–west directed SST-front, intersecting the Arabian coast at around 18°N. The effect of this abrupt SST change on the near-surface atmospheric stability, vertical momentum transfer, and on low-level winds is likely responsible for the striking similarity between the SST field and the near-surface wind speed (Fig. 7a); this result is also clear in Fig. 5c and explains the relatively lower signal of this jet on near-surface wind conditions. The effect of the large-scale oceanic circulation in the Arabian Sea, during the summer monsoon season, is also an important factor to take into account (Beal et al., 2013). Closer to the coast of Oman, lower SSTs are also seen northeast of $\sim$18°N, likely due to the effects of the coastal upwelling.

To investigate the regional vertical structure of the Oman CLLJ vertical across- and along-flow sections are shown in Fig. 8, following the (red and black) lines depicted in Fig. 1b. This is where the distinction between the Oman CLLJ and the Findlater jet becomes obvious. From the cross-flow cross-section (Fig. 8a), a low altitude, high wind-speed core with wind speeds in excess of 25 ms^{-1}, is clearly visible near the coast. This low-level jet is the Oman CLLJ, documented by Ranjha et al. (2013). Its core is found close to the coastline, and extends offshore to around 150 km. Potential-temperature contours (isentropes; black solid lines) show the subsidence inversion capping of the relatively cool MABL aloft. This inversion slopes upwards away from the coast towards the ocean, indicating a deepening of the MABL with an increasing offshore distance, a characteristic of a CLLJ. This slope of the MABL height (or inversion) provides the thermal wind structure that forces the coastal jet. The slope is a consequence of the weaker subsidence inversion (large-scale subsidence) and warmer SSTs away from the coast in the Arabian Sea (100–300 km offshore), and also a consequence of the secondary vertical circulation that appears around any semi-geostrophically balanced jet (Beardsley et al., 1987). The near-vertical isentropes close to the coast are a result of the considerably warmer air present over the strongly heated land mass, compared to the marine air over the ocean. The core of the Oman coastal jet is confined within the MABL, just below the capping inversion, at heights of around 500–600 m a.s.l. The MABL height is roughly around 600 m a.s.l., in agreement with the results by Ranjha et al. (2013). Above the capping inversion, higher potential temperatures and weaker winds are found. This case shows structures that are very similar to the typical northerly jet off the northern and central coast of California.

The second high wind-speed core (Fig. 8a), farther offshore, between 1200 m and 1500 m a.s.l., encompasses wind

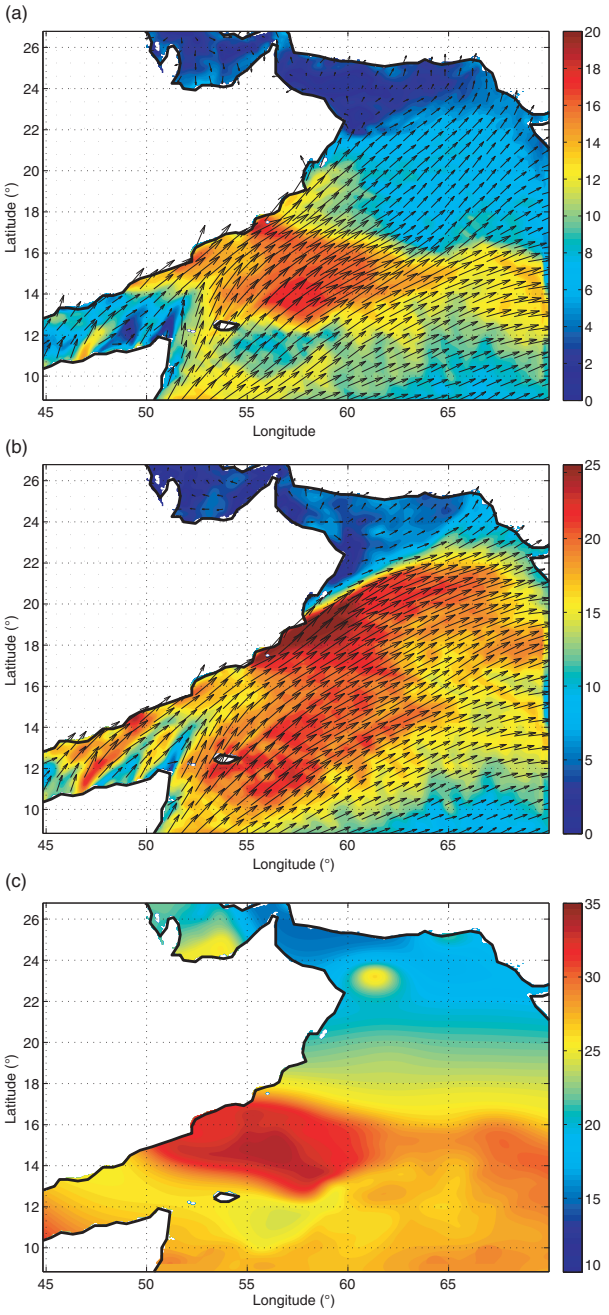

Fig. 7. Case-study horizontal fields from COAMPS® (2 July 2009 at 20:00 LT – 16:00 UTC) of (a) wind speed at 8 m (m s^{-1}) a.s.l., (b) wind speed at ~400 m a.s.l. (m s^{-1}), and (c) high-resolution SST (°C; from GHRSST) for the same day. The arrows represent the wind direction.

speeds in excess of 26 m s^{-1} at the jet core around ~550 km away from the coast. This wind-speed maximum resides inside a horizontal temperature inversion, in contrast to the CLLJ located below the sloping inversion closer to the coast. A detailed examination of the horizontal extent of this wind field reveals an area of separation between the two jets at around 350 km offshore. This second jet-like feature is in fact the Findlater (or Somali) jet, as documented by Findlater (1969a). It should be noted that the presence of two distinct but separated jet cores was not evident from the Oman CLLJ documented in Ranjha et al. (2013), using the coarse-resolution ERA-Interim data. The clear separation of the two jets was only possible with a higher resolution simulation. Figure 8b depicts the vertical along-flow section along the coast of Oman (red line in Fig. 1b), where the core of the Oman CLLJ is seen at a height of 500 m between 57° and 60°E. The tight stacking of the isentropes east of ~57–58°E shows the presence of the cool and denser marine air, capped by warm subsiding air, besides a considerably shallower MABL, where the wind speed increases.

4.2. *Summer characteristics of the Oman CLLJ*

The summer (JJA) seasonal CLLJ frequency of occurrence for 2009 obtained by applying the detection algorithm of Ranjha et al. (2013) to the 6-km modelled fields is shown in Fig. 9, along with ERA-Interim results. There is a general agreement in terms of CLLJ frequency of occurrence (above 70%) between the highly-resolved model results and the coarsely-resolved ERA-Interim data. However, the exact spatial distribution of the CLLJ occurrences is different in the two datasets. In the high-resolution model data (Fig. 9a), near-coast processes are resolved in much greater detail. The CLLJ frequency distribution of the high-resolution simulation is also shifted northeastwards towards Pakistan, compared to ERA-Interim (Fig. 9b). From Fig. 9a, the region with the highest CLLJ frequency starts at around 57°E and continues beyond the NE corner of the Oman coast into the mouth of the Gulf of Oman, whereas in ERA-Interim (Fig. 9b) it starts at around 56°E and towards NE it decreases much faster. This can be explained from the high-resolution modelled results presented in Fig. 7, where a SW pool of high SSTs stands in contrast to the relatively cooler NE waters. The presence of these high SSTs tends to reduce the coastal baroclinicity to the SW and thereby appears to have prevented the jet formation here. On the other hand, the cold SSTs to the NE strengthen the land–sea temperature contrasts and consequently increase the baroclinicity here. These cold SSTs can be linked to the positive feedback mechanism, whereby coast-parallel winds induce upwelling filaments, which in turn lead to colder surface waters and even stronger baroclinity, thereby strengthening the coastal jet. Also, since COAMPS® resolves small-scale wind and temperature features in greater detail, the majority of the modelled corner flow accelerations off the Horn of Africa are not classified as CLLJs within the high resolution modelled data (see Fig. 9a). In the ERA-Interim dataset, however, the coarse resolution accounts for a larger number of false positives in the same region (see Fig. 9b).

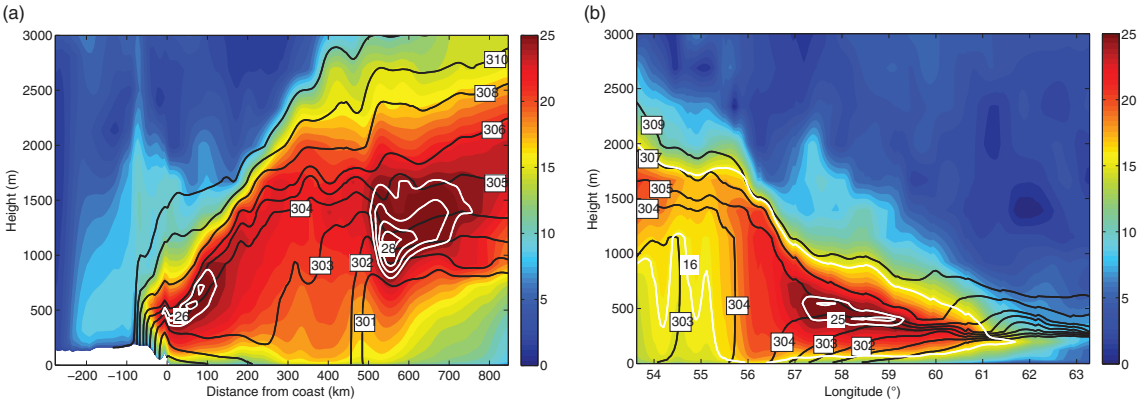

Fig. 8. Case-study vertical cross-sections from COAMPS® (2 July 2009 at 20:00 LT –16:00 UTC) of (a) cross-coast and (b) along-coast (see lines in Fig. 1b) of wind speed (m s^{-1}; shading and selected white lines with labels) and potential temperature (K; black lines with labels).

From Figs. 3 and 4, it is clear that the JJA season is associated with the highest wind speeds in the area, while May and September are transition months, associated with the beginning and end, respectively, of the peak-wind season. The monthly CLLJ spatial distribution and number of occurrences during the peak season months (June–August) and of the transition months (May and September), along with the monthly-mean wind-speed fields at roughly the core height, ~400 m a.s.l., are illustrated in Figs. 10 and 11, respectively.

During the summer period the wind speed (Fig. 10b, d, and f) increases along with the CLLJ frequency of occurrence (Fig. 9a, c, and e) from June to July, and both decrease to August. During June (Fig. 10b) the average jet wind-speed is almost 20 m s^{-1} and a jet-like feature has built up along the coast of Oman. This increase in wind speed and the associated jet-like features result in an increase of the CLLJ frequency to nearly 70% (Fig. 10a). Similarly, during July (Fig. 10d) the wind speed increases further to around 22 m s^{-1}, with a band of strong winds along the entire coast of Oman. This is reflected also as an area of high CLLJ occurrence (nearly 80%; Fig. 10c), where almost 25 d out of 31 feature coastal jet occurrences in the core jet area that extends eastwards towards the coasts of Pakistan and India. During August, the wind speed decreases to below 20 m s^{-1}, and the band of high wind speeds shifts further eastwards (Fig. 10f). This shift of the dominant wind pattern is seen in the corresponding CLLJ frequency of occurrence, where CLLJs are seen to occur somewhat eastwards (~70% occurrences; Fig. 10e) relative to July.

There is also a band of strong winds along the northern tip of Somalia, extending over the Socotra Island. This band remains almost the same, independent of the seasonal variability of the Oman CLLJ. However, despite encompassing mean wind speeds up to 25 m s^{-1} at ~400 m a.s.l., this region does not show any significant

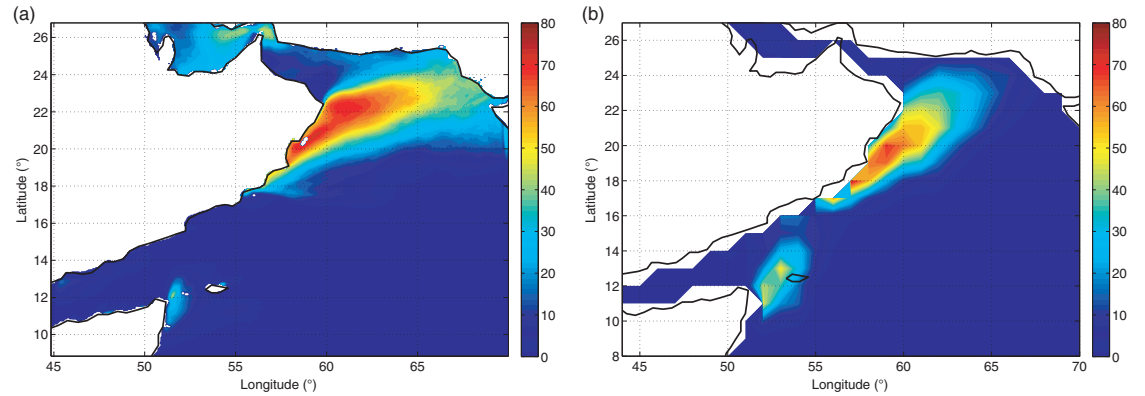

Fig. 9. CLLJ frequency of occurrence for JJA (%) (a) from COAMPS® results for the model inner domain (see Fig. 1b), and (b) from ERA-Interim.

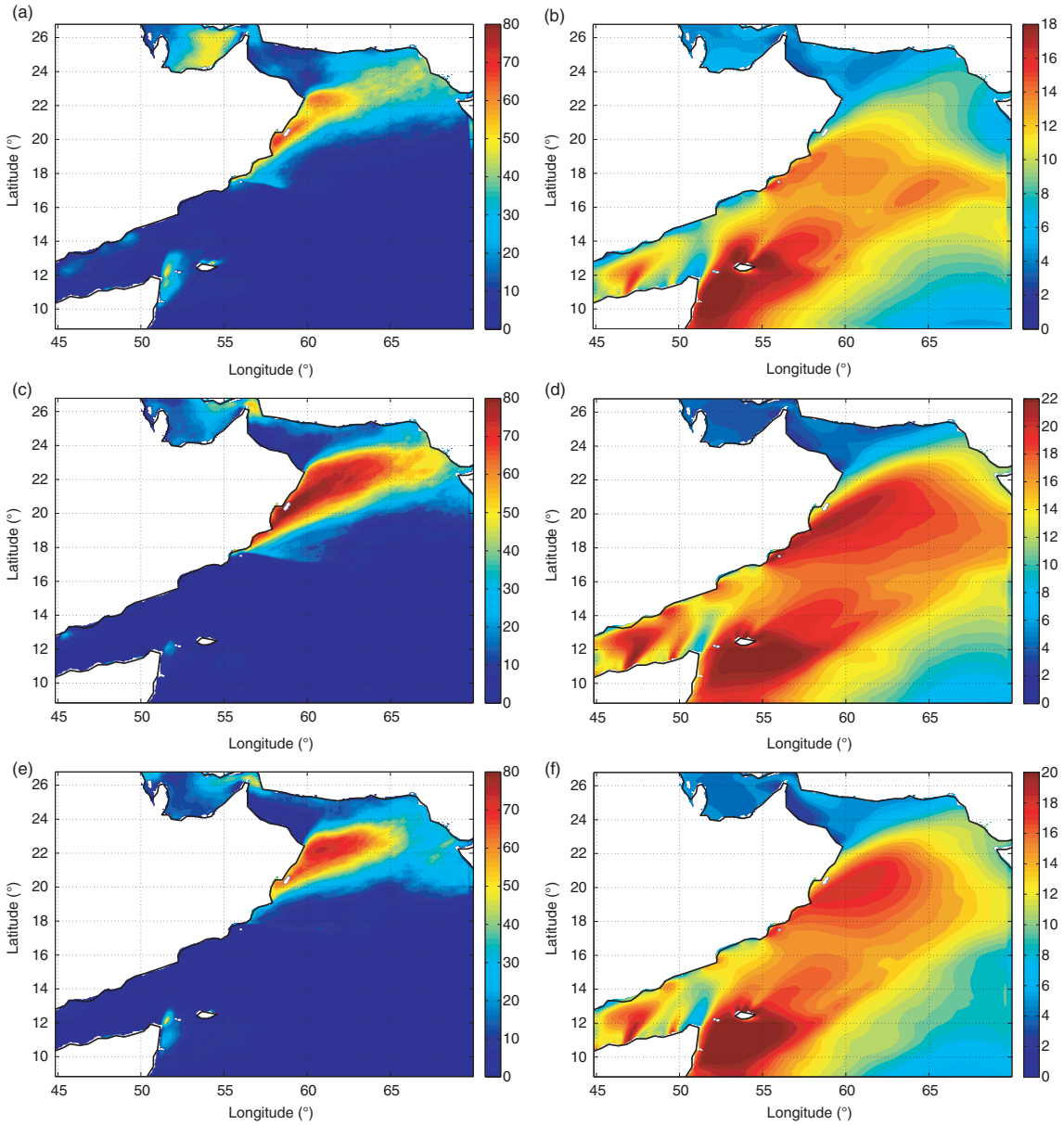

Fig. 10. Monthly (a, c and e) CLLJ frequency of occurrence (%), and (b, d and f) mean wind speed (contours) at 400 m a.s.l. (m s^{-1}), from COAMPS®, for (a and b) June, (c and d) July, (e and f) August. Note the different colour scale in the wind speed plots, in accordance with monthly varying strength.

CLLJ occurrence. As discussed earlier, these winds are a part of the large-scale Findlater jet circulation found farther offshore as well as higher aloft, in the vicinity of the Oman coast in the Arabian Sea (see Fig. 8a).

During the transitional months (Fig. 11), the monthly average frequency of occurrence is low and the mean wind speed at ~400 m a.s.l. is relatively weak, compared to the summer months: ~8 ms^{-1} in May and even weaker in September. The frequency of occurrence of CLLJ is low (lower in May) when compared to the summer months. Note that although the wind speed and the CLLJ occurrences are clearly lower off the coast of Oman, the strong winds well off shore, associated with the Findlater jet, prevail along the coast of Somalia in the Horn of Africa.

In addition to the horizontal fields shown in Figs. 10 and 11, the analysis is extended to highlight the Oman CLLJ characteristics (jet-height, wind-speed and wind-direction histograms) during the summer and transitional months (MJJAS), as well as during the JJA as a seasonal composite, as shown in Fig. 12. The CLLJ features for May (Fig. 12a),

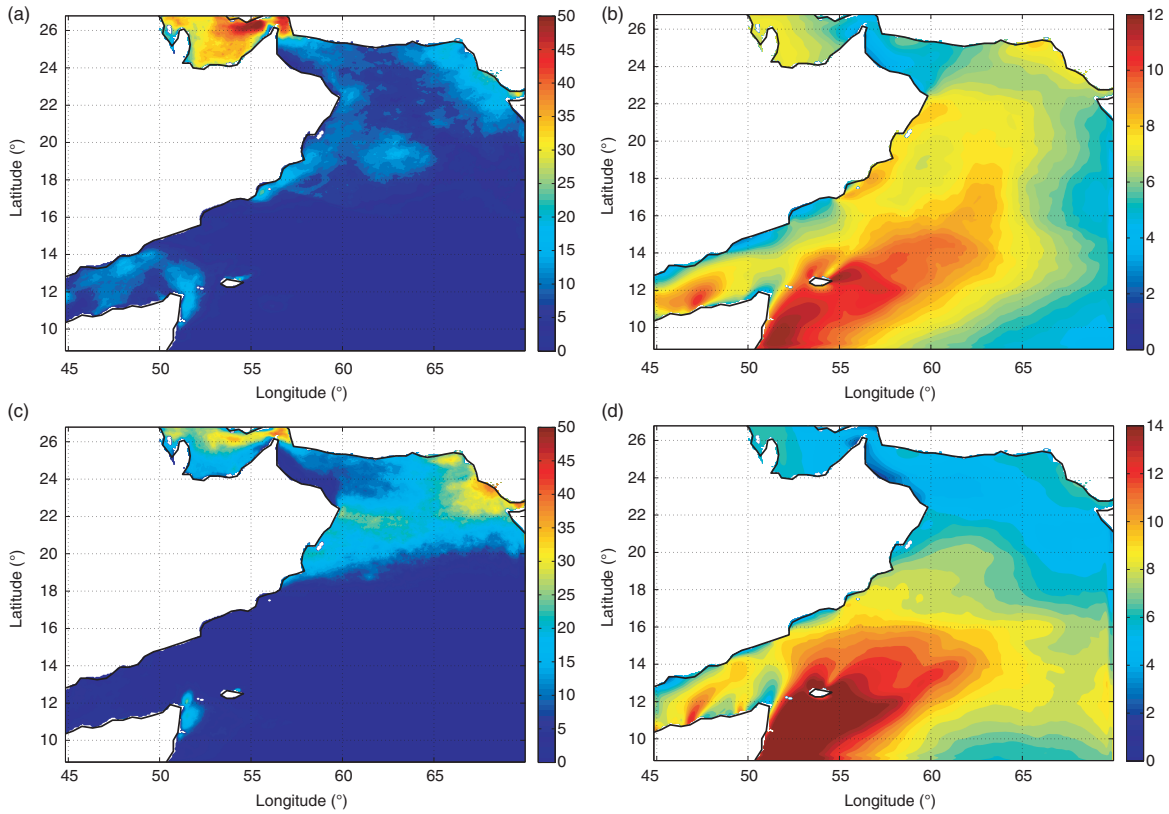

Fig. 11. Same as in Fig. 10 but for May (a and b) and September (c and d).

show variable jet heights, and the wind maxima are found at varying heights ranging mostly from 50 to 500 m a.s.l. The wind speed is relatively weak, with a dominant speed in the range of 6–12 ms^{-1}. A clue to the inconsistent wind-maxima height can be inferred from the wind direction, which is fluctuating between westerly to south–southwesterly. From the height-wind plot it is evident that during May, the CLLJs with highest wind speeds are found at lower heights, between 200 and 300 m a.s.l. In summary, the May CLLJs in 2009 are weak and low in height with varying flow directions.

During June (Fig. 12b), most CLLJs have wind speed maxima between 200 and 700 m a.s.l, with the highest occurrences between 300 and 400 m a.s.l. Wind speeds increased compared to May, with the highest concentration of jets ($\sim$60%) between 9 and 15 ms^{-1}, while nearly 20% are characterised by stronger winds, between 15 and 18 ms^{-1}. This is consistent with the height-wind plot, where the highest wind speeds are found at 300–400 m. The wind direction has less variability in June, compared to May, and is mostly from south–SW to SW.

Unlike the previous months, the July statistics in Fig. 12c show maximum wind speeds at higher altitudes, with 70% of the occurrences between 300 and 700 m, most of them between 400 and 500 m ($\sim$30%) a.s.l. Nearly 50% of the occurrences have wind speeds between 18 and 24 m s^{-1}, while another 15% have even higher wind speeds between 24 and 27 ms^{-1}. From the height-wind plot, CLLJs with wind speeds in excess of 25 ms^{-1} are found at heights between 400 and 500 m. These high wind speeds can be attributed to a dominant uniform SW coastal-parallel flow, less variable in direction than in June. August CLLJs in general (Fig. 12d) are fairly similar to the July ones, with the highest number of jet wind-speed maxima between 400 and 500 m with same wind direction. However, a detailed analysis reveals that the wind speed in August is slightly on the low side compared to July, in accordance with the horizontal wind pattern shown in Fig. 10. A composite of the prominent CLLJ characteristics for the JJA season is shown in Fig. 12f. The mean height of the jet core is between 400 and 500 m a.s.l., whereas the wind speed spans a broad range between 9 and 24 ms^{-1}. However, it is noticeable that a large number of CLLJs have wind speeds between 21 and 24 m s^{-1}. Furthermore, the wind direction is mostly from SW, as a response to the monsoon large scale synoptic forcing.

During September (Fig. 12e) nearly 55% of the CLLJ wind speed maxima are between 200 and 500 m heights.

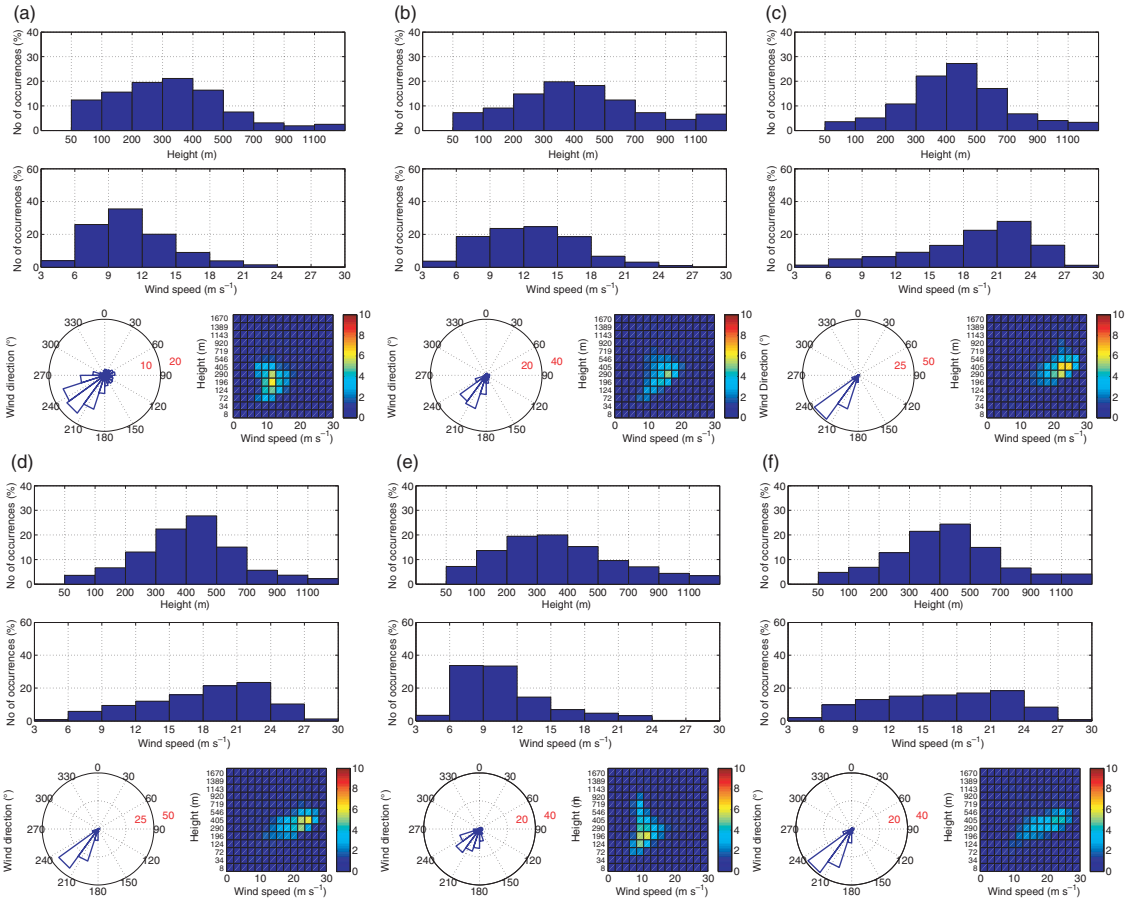

Fig. 12. CLLJ statistics for (a) May, (b) June, (c) July, (d), August, (e) September and (f) JJA, based on COAMPS® inner domain results for year 2009. Each panel comprises histograms of frequency of occurrence of CLLJ maxima height (m; top), wind speed (m s^{-1}; middle), direction (^{0}; lower left) and 2-D histogram of jet height and wind speed (%; lower right).

However, the wind speeds are on the low side, with around 70% of the occurrences between 6 and 12 ms^{-1}. This is corroborated by the height-wind speed plot, where most of the CLLJ occurrences have wind speeds of $\sim$10 ms^{-1}, within the 200–300 m interval. The wind-direction histogram provides the answer to the erratic characteristics of the September CLLJ. Like May, the wind pattern in September is highly variable, with the wind direction shifting between westerly to southerly, a situation which is not consistent with a coast-parallel flow, considering the orientation of the Oman coast. The characteristics of the September Oman CLLJ bear a close resemblance to those in May, in agreement with the earlier discussion in connection with Fig. 11. The CLLJs during May and September are relatively weaker, low in altitude, and with variable direction. The dominant-flow direction during these months accounts for the low wind speeds and are associated with the lower frequency of occurrence. Since the wind direction reverses seasonally, back and forth between SW to NE, May and September exhibit these transitions. The statistics presented here illustrate the situation in 2009, and the timing of these large-scale wind reversals varies from year to year, which can explain the seasonally broader distribution found in the ERA-Interim 31-yr climatology (Fig. 3b).

To further contrast the differences between the peak-season CLLJ months and the transitional months, Fig. 13 presents the probability density functions of the CLLJ heights and wind speeds (maxima) at the jet core for each of the May–September months, as well as for the JJA composite. July and August stand out as the months with the jet cores at higher altitudes, with the highest occurrences at around 400 m a.s.l., followed by June, where most of the occurrences take place between 300 and 400 m (Fig. 13a). May and September, however, have most of the CLLJ cores at lower heights, between 200 and 300 m. The wind-speed distribution (Fig. 13b) also demonstrates the clear differences within the months. The highest wind speeds are found in July, followed by August with a majority of occurrences at

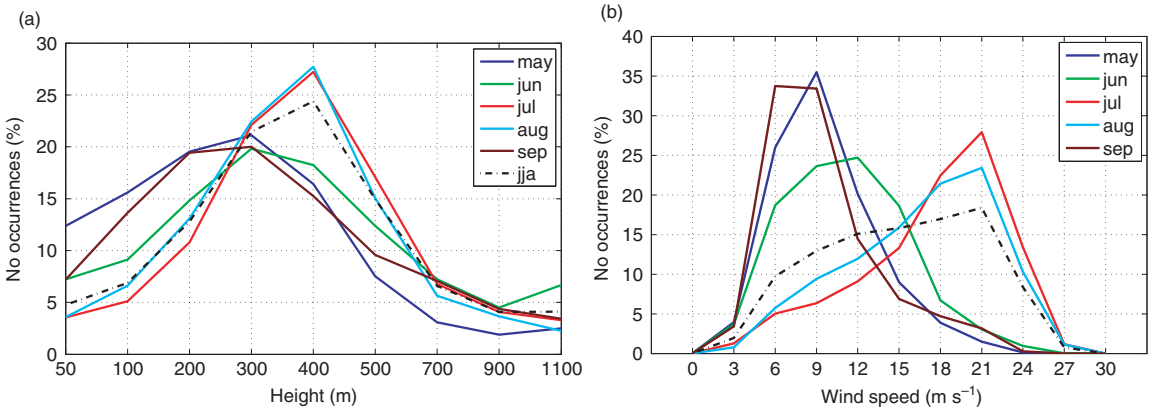

Fig. 13. Probability density functions for (a) height of CLLJ maxima and (b) wind speed for the May through September and for JJA from COAMPS®.

around 21 ms^{-1}. June, however, is characterised by weaker winds, compared to July and August, with the bulk of the occurrences between 9 and 12 ms^{-1}. May and September exhibit the lowest wind speeds (6–9 m s^{-1}) as transitions months.

The evolution of the daily mean wind speed at 8 and 400 m a.s.l. at point A (see Fig. 1b), from May to September, and the corresponding MSLP gradient between points L1 and H1 (see Fig. 1b), as well as the corresponding evolution of the daily mean number of occurrences from the inner domain for the same period, are shown in Fig. 14. The wind speeds, at 400 m and close to the surface (Fig. 14a), are highest between July and August, following the evolution of the synoptic forcing, with higher pressure gradients between the inland and offshore points during these months. The time series of the daily mean wind speed at the upper level correlates well with the corresponding MSLP gradient, with $r = 0.83$. The corresponding correlation coefficient with the wind speed at the lowest model level (8 m) is lower (0.73).

The evolution of the daily mean number of occurrences from May to September for the same period for the whole COAMPS® inner domain (Fig. 14b) is coherent with the wind speeds and pressure gradient time series, with a significant increase of the number of coastal jet occurrences during summer, particularly in July and August, with lower jet occurrences in the pre- and post-monsoon months. The role of the synoptic forcing on the wind speed evolution from May to September is clear from the correlation coefficients with the MSLP gradient. However, the wind speeds at point A are also driven by the strong coastal (mesoscale) pressure gradient due to the ocean–land thermal difference, which is borne out by the sub-monthly variations in the MSLP gradient.

The short-term MSLP-gradients are responsible for a diurnal cycle often displayed by CLLJ, because the temperature of the coastal landmass varies with insolation and with it the temperature gradient across the coast. Beardsley et al. (1987) presented a plausible explanation for the diurnal

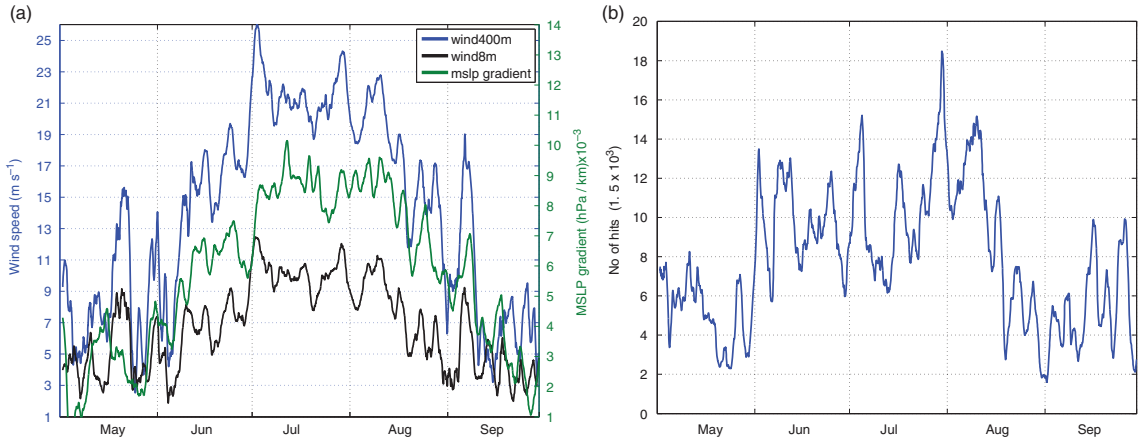

Fig. 14. Daily running average of (a) MSLP differences (hPa) between points L1 and H1 (see Fig. 1b), and wind speed at 8- and ~400 m a.sl. at point A (m s^{-1}) and (b) number of CLLJ counts for entire inner COAMPS® domain, with masked land, for May–September.

variation of the MABL structure in the near-shore region in a CLLJ area, and hence for the diurnal variation of coastal jets strength. During the night the temperature contrast between land and the ocean is small (or smaller, compared to day time), and the slope of the MABL capping inversion towards the coast is gentle and less pronounced. Therefore, close to the coast, during the night, the MABL winds are relatively weak. In the morning, when the sun starts to heat the land surface, the air destabilises, allowing for a penetration of the MABL air over land. At the same time, the slope of the inversion towards the coast increases, and the wind speed also increases, and the CLLJ becomes stronger, usually by late afternoon.

Figure 15 depicts the diurnal pattern of the Oman CLLJ, showing the monthly averaged diurnal cycles of the hourly MSLP gradient between points L2 and H2 (see Fig. 1b), for each of the MJJAS months during 2009, and of the corresponding evolution of the mean number of CLLJ occurrences in the COAMPS® inner domain. Regarding the pressure gradient (Fig. 15a) all months show similar diurnal patterns and amplitudes, but at different mean levels. The summer months (June to August) have the largest diurnal variations (amplitude) of MSLP gradient: around 4 Pa/Km), while May and September have slightly lower diurnal variations, as well as lower absolute pressure gradients. July has the highest MSLP gradient with a peak around 1.15 Pa/Km, followed by August and June, in line with the results in Fig. 14a. In all three summer months there is not exactly a peak of MSLP gradient. There is a broad plateau of the highest values, roughly from 16.00–1700 to 20.00–21.00 LT. After that, due to the night-time infrared radiation, the atmosphere over land cools and the pressure gradient decreases, starting to build again after sun rise.

During a 24-hour period the largest number of CLLJ occurrences (Fig. 15b) takes place later than the highest values of MSLP gradient. In June the peak of occurrences starts around midnight, and lasts, with very little variation (decrease), until early morning. In July, the peak of CLLJ occurrences is clearly defined and takes place at dawn, close to sunrise. During August the diurnal variation is similar to June, with a maximum value of CLLJ occurrences around 04.00 LT, but reaching the plateau of maximum values around 02.00 LT, lasting until sunrise with minor variations. In August the number of CLLJ occurrences is lower than in June, although the MSLP gradient is higher. The diurnal cycle of CLLJ occurrences during May and September is similar, with almost constant high values from 22.00 LT until early morning. In all months the minimum values of CLLJ occurrences occur around local noon. The lag between the MSLP gradient peak (or plateau or maximum value) and the maximum of CLLJ activity can be explained with the time-scale of the geostrophic adjustment, which is longer at this low latitude than at mid-latitude locations, due to the lower Coriolis force, and longer than the inertial period (at this location about 35h). Note also that the pressure gradient never crosses zero, although it comes close to zero in the morning hours during May, hence on average the pressure gradient forcing never reverses. Recall, however, that these are monthly averages and hence the pressure gradient may well have reversed on individual days. Since May and September has the lowest average pressure

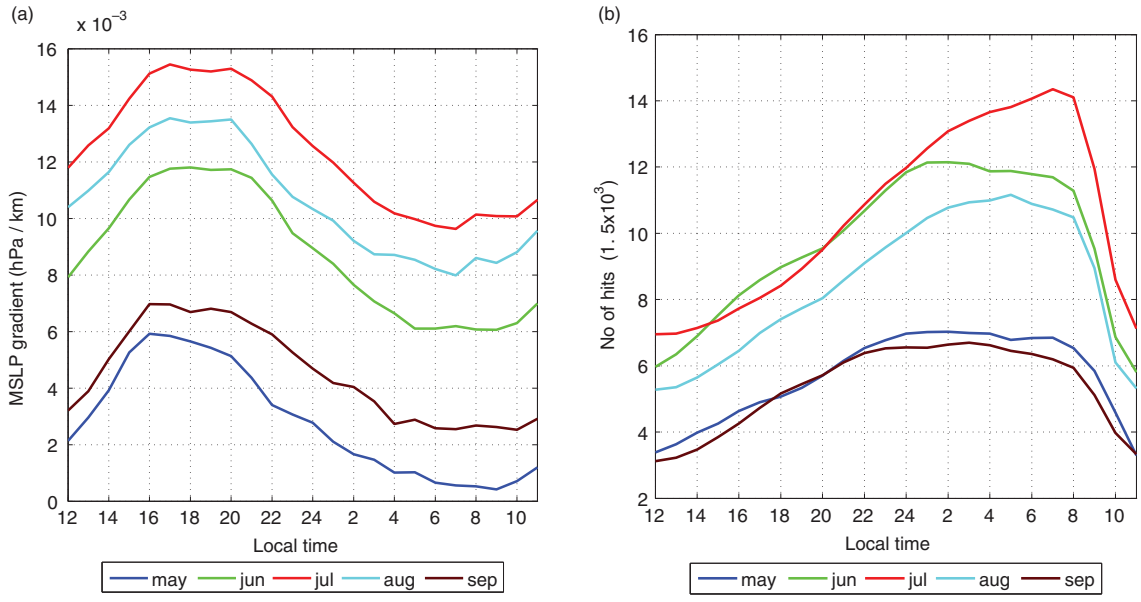

Fig. 15. Mean monthly diurnal cycles from COAMPS® for May through September of (a) MSLP gradient (hPa/km) between points L2 and H2 and (b) number of CLLJ counts for point A. See Fig. 1b for geographical references.

gradient, this explains the more variable wind directions during these months as the average minimum MSLP gradient is smaller.

Figure 16 illustrates the monthly averaged diurnal variation of the CLLJ height and strength (wind speed at the jet height) from the COAMPS® inner domain, also from May to September 2009. Unlike other coastal jets, like, for example the California CLLJ (e.g. Beardsley et al., 1987; Söderberg and Tjernström, 2002), in the Oman CLLJ the diurnal variations in the jet height and wind speed are weak or almost absent. Instead, the most pronounced diurnal variation appears in the CLLJ frequency of occurrence (deeper red colours in the figure). During the transitional months (Fig. 16a, b, i and j) there is a peak of occurrences from late afternoon through evening, roughly between 16:00–17:00 and 23:00–24:00 LT, while the minimum occurrence appears from mid-morning to noon or early afternoon, roughly between 08:00–09:00 and 12:00–13:00 LT. During these months the heights and strength of the CLLJ show a weak diurnal variation, with the CLLJ heights being most often located around 300 m, and the wind speeds around 8–10 ms^{-1}. However, the inter-diurnal variation is quite large, especially at the diurnal peak where CLLJ heights vary from less than 100 m to about 400 m. At the diurnal minimum, the heights are more often confined to around 300–400 m, with a slight tendency for a decreasing occurrence with increasing height. During July and August (Fig. 16e, f, g, and h) the diurnal variation signal is weaker but still present. The CLLJ heights and wind speeds are higher, compared to May and September, but the inter-diurnal spread is smaller. The whole diurnal cycle in the frequency of occurrence is pushed to slightly later, in line with Fig. 15b, with a maximum roughly from 17:00–18:00 persisting to 04:00–06:00 LT, roughly before local sunrise. In June (Fig. 16c and d) the diurnal variation is weaker than in May and July, with highest occurrences from 17.00 to around 24.00–01.00 LT. During summer months the minimum frequency of occurrence is later than in the transitional months, at 14:00–16:00 LT, but slightly more confined. Following a full diurnal cycle, during June to August, the lowest CLLJ heights seem to precede the maximum occurrences. The jet heights gradually increase somewhat to a maximum height that precedes the lowest frequency of occurrence value, and the drop back to lower CLLJ heights is faster than the increase during the evening and the night. On the other hand, the wind speed at the jet height is much higher than during the transitional months, consistently $\sim 21 \pm 2$ ms^{-1}. There is however a weak tendency for a low-wind period in the distribution. It must be taken into account that this analysis is based on cases qualified as CLLJ, and hence there must be occurrences when the coastal jet wind speed is weaker, down to ~ 8 ms^{-1} (slightly more common in August than in July). Interestingly, this appears only from noon to around 21.00, the part of the day when higher occurrences of CLLJ are expected, but not in the morning.

5. Summary and conclusions

In spite of its high frequency of occurrence as documented in Ranjha et al. (2013), the coastal jet along the SE coast of Oman had not been previously studied in detail. Here, the non-hydrostatic limited area model COAMPS® was used at 6-km resolution for a 5 months downscaling simulation, from May to September 2009, to analyse the mesoscale structure, spatial variability and temporal characteristics of the Oman CLLJ. The ECMWF ERA-Interim reanalysis was used both to provide a climatological background and as lateral boundary forcing to the COAMPS® simulations. A high-resolution SST dataset was used at the lower boundary. The model output was subjected to a filtering algorithm that efficiently isolates CLLJs from other low-level wind maxima (Ranjha et al., 2013) and the selected year, 2009, was found to be representative for the summer CLLJ by comparison to the 31 yr climatology from ERA-Interim. The COAMPS® high-resolution fields were then used to analyse the regional-scale wind speeds, pressure gradients and temperature patterns, as well as CLLJ occurrences.

After subjecting the mesoscale model data to the same CLLJ detection algorithm we also analysed the occurrence and characteristics of the Oman coastal jet. Based on the wind speed and the frequency of occurrence maps, it was shown that an area of strong CLLJ activity exists around 18°N 57°E, extending northeastwards along the SE coast of Oman. This is a region of high coastal baroclinicity, giving rise to a sharp cross-coast pressure gradient and to the correspondent jet-like flow along the coast.

The Oman coastal jet is unique in terms of its very high frequency of occurrence, geographic location, direction, and synoptic forcing. All other regions where CLLJ are found are located on the west coast of sub-tropical continents, along eastern boundary currents (Ranjha et al., 2013) and the CLLJ direction is equatorward. The Oman CLLJ is found on an east coast moving away from the equator. The link of the Oman CLLJ to the South Asia Monsoon and to the Findlater jet (Findlater, 1969a, 1969b) also makes it distinct from other coastal jets. Whereas other regions with CLLJ are strongly governed by the position of the sub-tropical high-pressure systems, here the monsoon circulation provides the large scale setting for the CLLJ.

A clear separation between the Findlater jet and the Oman CLLJ was shown (Figs. 8a and 10), possible only due to the mesoscale high-resolution simulation used here. The Findlater jet is found farther offshore and at a higher altitude (~ 1500 m), relative to the Oman jet. While the Oman CLLJ is a consequence of local coastal baroclinicity

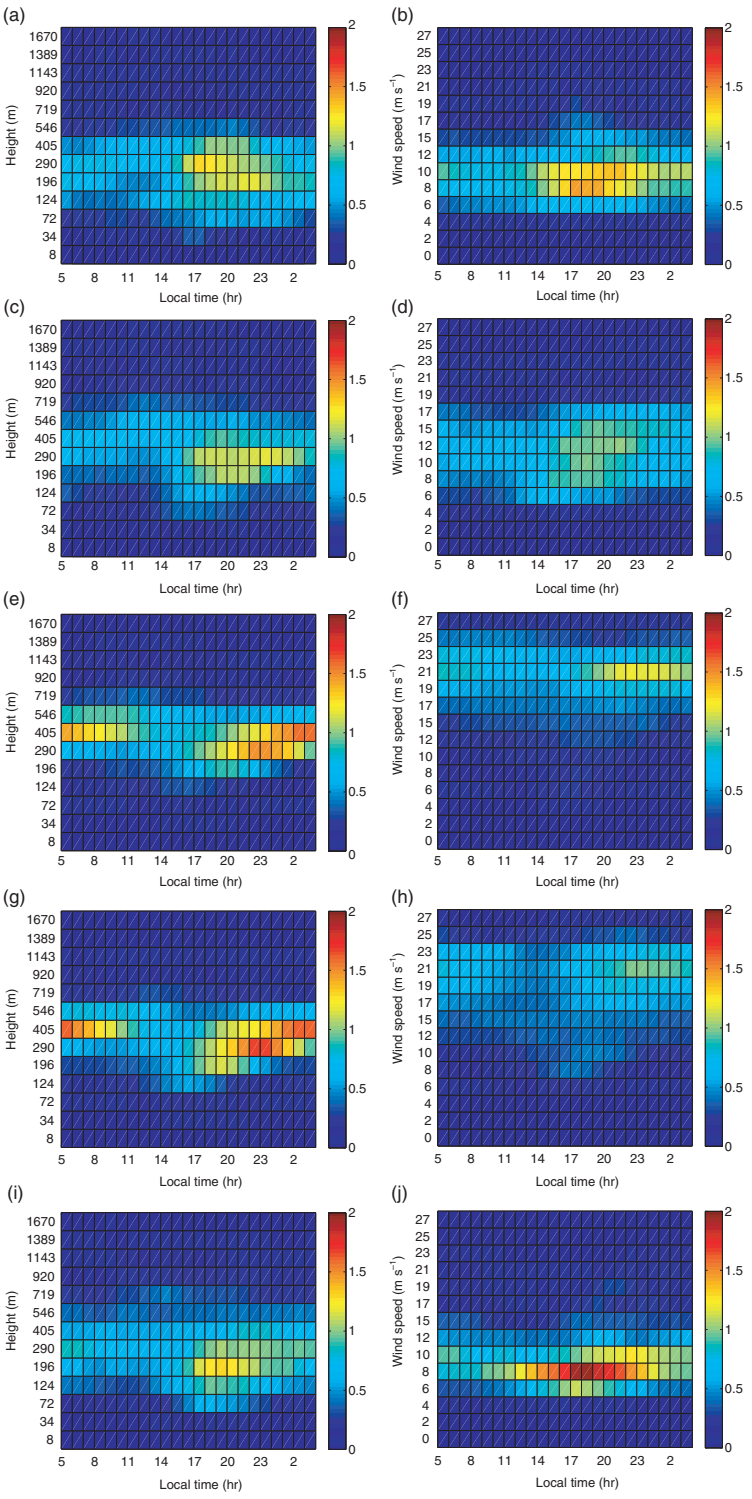

Fig. 16. Two-dimensional probability of the mean monthly diurnal cycles of (a, c, e, g, i; left column) jet heights and (b, d, f, h, j; right column) wind speed for (from top to bottom) May, June, July, August and September.

due to differential land–sea heating, the Findlater jet is forced by the large-scale cross-equatorial pressure gradients and the resulting larger scale circulation. The separation of the Oman CLLJ as an individual low-level coastal flow, differing from the Somali jet in its smaller-scale features and mesoscale forcing, is an important result. Further detailed

analysis and modelling is required to ascertain if there are any feedbacks or other connections between the two jets. This question is, beyond the scope of the present study.

Analysis of the modelled monthly averaged fields revealed that the Oman CLLJ activity is highest during July, with a maximum occurrence rate of $\sim$80%, followed by August and June at 75 and 70%, respectively. July also exhibits the strongest wind speeds (up to 27 ms^{-1}) at the jet core, and a consistent SW coast-parallel flow. May and September have weaker wind speeds and lower CLLJ activity, and can be seen as transition months. This is attributed to the forcing from the seasonal wind reversals in the Arabian Sea region associated with the monsoon flow: SW (NE) winds during summer (winter). May and September can be considered as a transition months to the onset of summer flow and the winter flow, respectively, with the associated wind reversal. The summer months, particularly July and August (Figs. 10 and 11), have stronger jet wind-speed maxima, and a more well-defined and steady coast parallel flow from the SW, compared to the transitional months.

The Oman CLLJ exhibits a well-defined diurnal variability in terms of frequency of occurrence, with the highest CLLJ occurrences taking place during dawn and early morning hours before sunrise, while the maximum MSLP gradient at the coast takes place during late afternoon. This time lag between the maximum pressure gradient and the maximum CLLJ occurrences can, in principle, be explained by the time-scale of the geostrophic adjustment at such low latitude, where the Coriolis force is low. On the other hand the diurnal cycle of the Oman CLLJ jet heights and, particularly, of the wind speed at the jet height, is not very well defined, particularly the latter, and do not necessarily follow the coastal jet occurrences (and are not in line with the findings of Beardsley et al., 1987). At this latitude the inertial period (geostrophic adjustment time) is longer than the diurnal cycle, which helps explain both the unusually high and persistent wind speed in the Oman CLLJ and the lack of a pronounced wind speed diurnal cycle. One may see this as a continued but delayed acceleration of the jet, even after the forcing has started to decrease as the inland heating has stopped and cooling has started. Then the following heating cycle starts, and the forcing increases again before the jet has had time to decelerate appreciably from the action of surface friction. The diurnal cycle of the MSLP gradient does typically not cross zero (Fig. 15a). Hence, even if the baroclinic forcing becomes small during the night and morning, there is no forcing, except the surface friction, that can slow down the jet appreciably. Thus, the effects from 1 d baroclinic forcing persist through the night and the next day's CLLJ starts somewhat stronger than the previous and so on, until surface friction balances the mesoscale pressure gradient forcing. The interaction of the Findlater jet above with the Oman CLLJ, and the possibility of momentum diffusion between them, with impact on the diurnal cycle, should also not be ruled out.

Some future suggestions for a deeper understanding of the Oman CLLJ can be outlined. More atmospheric *in-situ* observations of the coastal region are essential, both for describing the detailed structure of the jet and for corroborating the model simulations. The investigation reported here has demonstrated the important inter-linkage between atmospheric and oceanic processes affecting the CLLJ. Since our present knowledge of the oceanographic state of the Arabian Sea is sparse, improved marine surveys of this area would yield significant benefits for coming investigations of the Oman CLLJ. Combined atmosphere–ocean field campaigns would therefore contribute significantly to a deeper understanding of the Oman CLLJ and its connections and feedbacks with the Somali jet and with the south-Asia Monsoon. During the current investigation, the model runs were forced with daily high resolution SSTs (GHRSST), since interpolating from the coarser ERA-Interim SST to the COAMPS® domains resulted in unrealistic SST gradients (not shown). Studies on the importance of spatial and temporal small-scale SST variations, as well as the effects of coastal topography variations, on the variability and structure of the Oman CLLJ are also remaining challenges. Further dedicated research on the diurnal cycle on the Oman CLLJ and on its relation with the Findlater jet is also needed.

6. Acknowledgements

The authors are grateful to the Marine Meteorology Division of the Naval Research Laboratory, Monterey, for granting access to the COAMPS® and to the European Centre for Medium-range Weather forecasts for providing the ERA-Interim data. The simulations were performed on Triolith at the National Supercomputer Centre in Linköping, Sweden, and we are grateful for their support. We are also grateful to Peter Lundberg for valuable comments on the manuscript. R. Ranjha acknowledges support from the Higher Education Commission of Pakistan, while A. Semedo and R. M. Cardoso acknowledge support from the SHARE project funded by the Portuguese Foundation for Science and Technology (FCT – *Fundação para a Ciência e Tecnologia*, Portugal).

References

Annamalai, H., Slingo, J. M., Sperber, K. R. and Hodges, K. 1999. The mean evolution and variability of the Asian summer monsoon: comparison of ECMWF and NCEP-NCAR reanalyses. *Mon. Weather Rev.* **127**(6), 1157–1186.

Atlas, R., Hoffman, R. N., Ardizzone, J., Leidner, S. M., Jusem, J. C. and co-authors. 2011. A cross-calibrated, multiplatform ocean surface wind velocity product for meteorological and oceanographic applications. *Bull. Am. Meteorol. Soc*. 92, 157–174.

Beal, L. M., Hormann, V., Lumpkin, R. and Foltz, G. R. 2013. The response of the surface circulation of the Arabian Sea to monsoonal forcing. *J. Phys. Oceanogr*. **43**, 2008–2022.

Beardsley, R. C., Dorman, C. E., Friehe, C. A., Rosenfield, L. K. and Winant, C. D. 1987. Local atmospheric forcing during the Coastal Ocean dynamics experiment 1: a description of the marine boundary layer and atmospheric conditions over a northern California upwelling region. *J. Geophys. Res*. **92**, 1467–1488.

Brost, R. A., Wyngaard, J. C. and Lenschow, D. H. 1982. Marine stratocumulus layers. Part I: mean conditions. *J. Atmos. Sci*. **39**, 800–817.

Burk, S. D. and Thompson, W. T. 1996. The summertime low-level jet and marine boundary layer structure along the California coast. *Mon. Weather Rev*. **124**, 668–686.

Capet, X. J., Marcheiello, P. and McWilliams, J. 2004. Upwelling response to coastal wind profiles. *Geophys. Res. Lett*. **31**, L13311.

Chao, S. 1985. Coastal jets in the lower atmosphere. *J. Phys. Oceanogr*. **15**, 361–371.

Collins, C., Reason, C. J. C. and Hermes, J. C. 2012. Scatterometer and reanalysis wind products over the western tropical Indian Ocean. *J. Geophys. Res*. **117**, 1–16. DOI: 10.1029/2011jc007531.

COMET. 2004. Low-level coastal jets. Online at: http://www.meted.ucar.edu/mesoprim/coastaljets/

Cui, Z., Tjernstrom, M. and Grisogono, B. 1998. Idealized simulations of atmospheric coastal flow along the central coast of California. *J. Appl. Meteorol*. **37**, 1332–1363.

Currie, R. I. 1992. Circulation and upwelling off the coast of southeast Arabia. *Oceanol. Acta*. **15**(1), 43–60.

Dee, D. P., Uppala, S. M., Simmons, A. J., Berrisford, P., Poli, P. and co-authors. 2011. The ERA-interim reanalysis: configuration and performance of the data assimilation system. *Q. J. Roy. Meteorol. Soc*. **137**, 553–597.

Donlon, C., Robinson, I., Casey, K. S., Vazquez-Cuervo, J., Armstrong, E. and co-authors. 2007. The global ocean data assimilation experiment high resolution sea surface temperature pilot project. *Bull. Am. Meteorol. Soc*. **88**(8), 1197–1213.

Fennel, W. and Lass, H. U. 2007. On the impact of wind curls on coastal currents. *J. Mar. Syst*. **68**, 128–142.

Findlater, J. 1969a. A major low level current near the Indian Ocean during northern summer. *Q. J. Roy. Meteorol. Soc*. **95**, 362–380.

Findlater, J. 1969b. Inter-hemispheric transport of air in the lower troposphere over the western Indian Ocean. *Q. J. Roy. Meteorol. Soc*. **95**, 400–403.

Findlater, J. 1971. Mean monthly air flow at low levels over the western Indian Ocean. *Geophys. Memo*. **115**, 53.

Hodur, R. M. 1997. The Naval Research Laboratory's Coupled Ocean/Atmosphere Mesoscale Prediction System (COAMPS). *Mon. Weather Rev*. **125**, 1414–1430.

Hodur, R. M. and Doyle, J. D. 1999. The coupled ocean/atmosphere mesoscale model prediction system (COAMPS). In: *Coastal Ocean Prediction* (ed. C. N. K. Mooers). Coastal and Estuarine Studies, Vol. 56, American Geophysical Union, Washington, DC, pp. 125–155.

Holt, T. R. 1996. Mesoscale forcing of a boundary layer jet along the California coast. *J. Geophys. Res*. **101**, 4235–4254.

Houze, R. A., Jr., Wilton, D. C. and Smull, B. F. 2007. Monsoon convection in the Himalayan region as seen by the TRMM precipitation radar. *Q. J. Roy. Meteorol. Soc*. **133**, 1389–1411.

Izumo, T., Montégut, C. B., Luo, J.-J., Behera, S. K., Masson, S. and co-authors. 2008. The role of the western Arabian Sea upwelling in Indian Monsoon rainfall variability. *J. Clim*. **21**, 5603–5623.

Kalnay, E. C., Kanamitsu, M., Kistler, R., Collins, W., Deaven, D. and co-authors. 1996. The NCEP/NCAR 40-year reanalysis project. *Bull. Am. Meteorol. Soc*. **77**(3), 437–471.

Koracin, D. and Dorman, C. 2001. Marine atmospheric boundary layer divergence and clouds along California in June 1996. *Mon. Weather Rev*. **129**, 2040–2055.

Nuss, W. A., Bane, J., Thompson, W., Dorman, C., Ralph, M. and co-authors. 2000. Coastally trapped wind reversals: a new level of understanding from the experiment on coastally trapped disturbances. *Bull. Am. Meteorol. Soc*. **81**, 719–743.

Pant, G. B. and Kumar, K. R. 1997. *Climates of South Asia*. Wiley, Chichester, UK, 320 pp.

Parish, T. 1982. Barrier winds along the Sierra Nevada mountains. *J. Appl. Meteorol*. **12**, 925–930.

Parish, T. R. 2000. Forcing of the summer low-level jet along the California coast. *J. Appl. Meteorol*. **39**, 2421–2433.

Rahn, D. A. and Parish, T. R. 2007. Diagnosis of the forcing and structure of the coastal jet near Cape Mendocino using in situ observations and numerical simulations. *J. Appl. Meteorol. Clim*. **46**, 1455–1468.

Ranjha, R., Svensson, G., Tjernström, M. and Semedo, A. 2013. Global distribution and seasonal variability of coastal low-level jets derived from ERA-Interim reanalysis. *Tellus A*. **65**, DOI: 10.3402/tellusa.v65i0.20412.

Rijo, N., Lima, D. C. A., Semedo, A., Miranda, P. M. A., Cardoso, R. and co-authors. 2014. The Iberian Peninsula low-level coastal jet: climatology and case study analysis. In: *Proceedings 10th Jornadas do Mar*, November 11–14, 2014, Lisbon.

Risien, C. M. and Chelton, D. B. 2008. A global climatology of surface wind and wind stress fields from eight years of QuikSCAT Scatterometer data. *J. Phys. Oceanogr*. **38**, 2379–2413.

Small, C. and Nicholls, R. J. 2003. A global analysis of human settlement in coastal zones. *J. Coastal Res*. **19**, 584–599.

Soares, P. M. M., Cardoso, R., Semedo, A., Chinita, M. and Ranjha, J. R. 2014. The Iberian Peninsula coastal low level jet. *Tellus A*. **66**. DOI: 10.3402/tellusa.v66.22377.

Söderberg, S. and Tjernström, M. 2002. Transitions in supercritical flows along mountainous coastlines: on the diurnal cycle. *J. Atmos. Sci*. **59**, 2615–2624.

Ström, L., Tjernström, M. and Rogers, D. P. 2001. Observed dynamics of topographically forced flow at Cape Mendocino during coastal waves 1996. *J. Atmos. Sci*. **58**, 953–977.

Tjernström, M. 1999. Sensitivity of coastal atmospheric supercritical flow to ambient conditions. *Tellus A*. **51**(5), 880–901.

Tjernström, M. and Grisogono, B. 2000. Simulations of supercritical flow around points and capes in the coastal atmosphere. *J. Atmos. Sci.* **57**, 108–135.

Tjernström, M. and Koračin, D. 1995. Modeling the impact of marine stratocumulus on boundary layer structure. *J. Atmos. Sci.* **52**, 863–878.

Ullah, K. and Gao, S. T. 2012. Moisture transport over the Arabian Sea associated with summer rainfall over Pakistan in 1994 and 2002. *Adv. Atmos. Sci.* **29**(3), 501–508.

Warner, T. T. 2004. *Desert Meteorology*. Cambridge University Press, Boston, MA, 595 pp.

Webster, P. J., Magana, V. O., Palmer, T. N., Shukla, J., Tomas, R. A. and co-authors. 1998. Monsoons: processes, predictability, and the prospects for prediction. *J. Geophys. Res.* **103**, 14451–14510.

Winant, C. D., Dorman, C. E., Friehe, C. A. and Beardsley, R. C. 1988. The marine layer off northern California: an example of supercritical channel flow. *J. Atmos. Sci.* **45**, 3588–3605.

Zemba, J. and Friehe, C. A. 1987. The marine boundary layer jet in the coastal ocean dynamics experiment. *J. Geophys. Res.* **92**, 1489–1496.